


## Interpretation of recent form factor data in terms of an advanced representation of baryons in space and time

Egle Tomasi-Gustafsson <sup>\*</sup>*DPhN, IRFU, CEA, Université Paris-Saclay, 91191 Gif-sur-Yvette Cedex, France*Simone Pacetti <sup>†</sup>*Dipartimento di Fisica e Geologia, and INFN Sezione di Perugia, 06123 Perugia, Italy*

(Received 28 May 2022; accepted 12 September 2022; published 21 September 2022)

Data on electromagnetic form factors of proton, neutron, and  $\Lambda$  from annihilation and scattering reactions are collected and interpreted in the frame of a generalized picture of the internal structure of baryons which holds in space-like and time-like regions. It is shown that these data give an insight into the spatial structure of the baryon for distances 100 times smaller than the baryon size and, in the time-like region, a vision of the time evolution of the hadronic matter for times up to  $10^{-25}$  s, that is two orders of magnitude shorter than the time taken by the light to cross the volume of a proton. In the proposed interpretation, the electric form factor of the proton in the space-like region cannot cross zero, but vanishes or stays very small, as an extrapolation of the data seems to show. In the time-like region specific structures appearing in the data give evidence of the dominance of the quark-diquark underlying dynamics in a well-determined time interval during the evolution of the system.

DOI: [10.1103/PhysRevC.106.035203](https://doi.org/10.1103/PhysRevC.106.035203)

### I. INTRODUCTION

Electromagnetic form factors (FFs) contain essential information on the internal structure of hadrons and their theoretical and experimental investigation constitutes a basic tool in the field of intermediate energy physics. In a parity-conserving and time-reversal-invariant theory a particle of spin  $S = 1/2$  is characterized by two FFs, electric ( $G_E$ ) and magnetic ( $G_M$ ), that are functions of one variable only (for a review see Ref. [1]). The information of FFs is accessible through elementary scattering and annihilation reactions, assuming one photon exchange. The FF values are extracted from the data on differential cross section and polarization observables, after correcting, in particular, for radiative corrections.

The polarization of the recoil proton in processes of elastic scattering of longitudinally polarized electrons on an unpolarized proton target,  $\vec{e}^- + p \rightarrow e^- + \vec{p}$  (where the vector symbol stands for polarized particle), provides the information on FFs in the space-like region of transferred momenta, namely at  $q^2 < 0$ , being  $q$  the four-momentum of the virtual photon. This method, suggested by Akhiezer and Rekalov at the end of the 1960s [2,3] was applied only recently, due to the development of high duty cycle electron machines, large acceptance detectors, and hadron polarimeters in the GeV region. The results on the ratio of the electric to magnetic FF were very precise as expected, due to the sensitivity of the method to the small electric contribution. Surprisingly,

they showed that this ratio is not constant, but decreases almost linearly with  $Q^2 = -q^2$ , eventually crossing zero around  $Q^2 \simeq 9 \text{ GeV}^2$ .

In the time-like region, accessible through annihilation reactions, regular oscillations were highlighted in Ref. [4] considering the precise data collected by the BABAR experiment [5,6] on the proton generalized FF, later on confirmed by the BESIII experiment in Refs. [7,8]. The BESIII Collaboration published also the first individual determination of the moduli of the electric and magnetic proton FF in the time-like region [7], and unique data on the neutron FF. These data, once analyzed similarly to the proton case, revealed the presence of regular oscillations, but shifted by a phase with respect to the proton oscillations [9].

The purpose of this work is to analyze and interpret the recent data obtained on one side in the time-like region on neutron, proton, and hyperons most recently by the BESIII Collaboration [7,8], but also by the BaBar [5,6] and CMD [10] Collaborations, and on the other side in the space-like region mostly by the GEP Collaboration [11], in the framework of a model suggested ten years ago in Ref. [12]. The basic assumption of the model is that the center volume of the hadron is electrically neutral due to the strong gluonic field. This assumption has two principal effects: to induce a screening which decreases the electric FF with respect to the magnetic one, and to favor the development of a diquark configuration during the evolution of the system from the quark creation to the hadron formation. These features should be present in both space-like and time-like regions, although the physical interpretation of FFs is different in these domains.

In the space-like region, FFs have a clear interpretation in nonrelativistic approximation, where they are the Fourier

<sup>\*</sup>egle.tomasi@cea.fr<sup>†</sup>simone.pacetti@unipg.it

transforms of the electric charge and magnetic spatial density distributions. This holds also in the Breit system, which is defined as the reference frame where the energy of the virtual photon is zero, so that its four-momentum becomes  $q = (0, q_x, q_y, q_z)$ . Therefore in the space-like region, FFs contain information related to the baryon spatial densities at the scale defined by the four-momentum, which has only three vector components.

In the time-like region, the privileged system is the center of mass system (CMS), where the three-momentum is zero, i.e.,  $q = (q_0, 0, 0, 0)$ . Only the time component of the transferred momentum plays a role. FFs in the time-like region cannot bring any spatial information. Therefore, FFs that parametrize the cross section of the process  $e^+e^- \rightarrow \bar{p}p$ , describe the time evolution of the charge created at the annihilation point until the formation of the hadron pair. Eventually, this scale can be associated to the distance of the centers of the forming hadrons.

In order to formalize these concepts, a generalized definition has been proposed in Ref. [12] and further developed in Ref. [13]. Form factors are functions of  $q^2$  only, therefore it is possible to define a relativistic invariant in the following way:

$$F(q^2) = \int_{\mathcal{D}} d^4x e^{iq_\mu x^\mu} \rho(x), \quad q_\mu x^\mu = q_0 t - \vec{q}\vec{x}, \quad (1)$$

where  $\rho(x) = \rho(t, \vec{x})$  can be understood as the space-like distribution of the electric charge in a space-time volume  $\mathcal{D}$ .

In the scattering channel,  $ep \rightarrow ep$ , and in the Breit frame, we recover the usual definition of FFs  $F(q^2) = F(-\vec{q}^2)$ , having no energy transfer.

In the annihilation channel and in CMS we have

$$F(q^2) = \int_{\mathcal{D}_t} dt e^{i\sqrt{q^2}t} \int_{\mathcal{D}_x} d^3\vec{x} \rho(x) = \int_{\mathcal{D}_t} dt e^{i\sqrt{q^2}t} \mathcal{Q}(t), \quad (2)$$

where  $\mathcal{Q}(t)$  describes the time evolution of the charge distribution in the time domain  $\mathcal{D}_t$ , obtained after integration of the space-time distribution  $\rho(x)$  over the spatial domain  $\mathcal{D}_x$ , with  $\mathcal{D} = \mathcal{D}_t \cup \mathcal{D}_x$ .

This means that experimentally we have access to the projections of the generalized function on the space and on the time axis, in the Breit system and in CMS, respectively.

In the next section we recall the main features of the model of Ref. [12]. In Sec. III the space-like data are presented as a function of the internal spatial dimension as seen by the virtual photon, while the time-scale is illustrated in Sec. IV for the time-like data of nucleons and hyperons. In Sec. V a remarkable correlation among these FFs is discussed.

## II. DESCRIPTION OF THE SCATTERING AND ANNIHILATION PROCESSES

The nucleon description in terms of constituent quarks or vector dominance models assumes that the three colored valence quarks are surrounded by a neutral sea of quark-antiquark pairs and gluons. The model of Ref. [12] gives a different picture based on studies of the structure of quantum chromodynamics (QCD) vacuum and gluon condensate [14].

The center volume of the nucleon is assumed to be chromoelectrically neutral, due to the strong gluonic field that creates

a gluon condensate, with a randomly oriented chromomagnetic field [14]. At very small distances the gluon field as well as the chromoelectric field increases, inducing a screening effect that acts on the electric FF, leaving the magnetic distribution unchanged, similarly to the Coulomb field in a plasma. The magnetic distribution is expected to follow a  $Q^2$  dipole dependence, according to the scaling rules of QCD, while it can be shown that the electric distribution is suppressed by an extra factor of  $1/Q^2$ .

In the region of strong chromoelectromagnetic field, due to stochastic averaging, the color quantum number does not play any role. Therefore, due to the Pauli principle, quarks of the same flavor,  $uu$  for proton and  $dd$  for neutron, move away from the central region and one of them is attracted by the remaining quark,  $d$  in the proton and  $u$  in the neutron, forming a diquark. As the system expands and cools down, the strength of the gluon field decreases and the quark color degree of freedom is restored. This step is driven by the balance of the electric attraction force and the stochastic force of the gluon field. It is predicted to occur at a scale of 0.2–0.3 fm. At larger distances the gluon energy feeds the process of ‘dressing’ the quarks, which convert into constituent quarks.

The hadron formation in  $e^+e^-$  annihilation can also be described through three main steps in terms of evolution in time. In order to create the hadron-antihadron pair, the energy at the  $e^+e^-$  annihilation, concentrated in a small volume, should be at least equal to or larger than the threshold energy,  $E_{Th} = 2M_h$  ( $M_h$  being the hadron and antihadron mass). Then,  $q\bar{q}$  pairs are created by the vacuum fluctuations, with the same probability independently on flavor. However, due to the uncertainty principle, the time associated with the  $q\bar{q}$  pair depends on their mass and hence on the flavor, the heavier the  $q\bar{q}$  pair, the shorter the formation time. This affects the probability to create a hadron-antihadron pair, which requires for the  $p\bar{p}$  final channel, that two pairs  $u\bar{u}$  and one pair  $d\bar{d}$  are created in a space-time volume of dimensions  $[\hbar/(2M_h)]^3 \simeq (0.1 \text{ fm})^3$ . Below the physical threshold one expects that a system, constituted by at least three bare quark-antiquark pairs, is formed. This system, with the quantum numbers of the photon, can be considered point-like and colorless, due to the screening of the strong chromoelectromagnetic field. Similarly to the space-like picture, the Pauli principle applies to the two identical quarks, one of them is attracted by the remaining quark, forming a diquark. The system expands and cools down, the quarks absorb gluons and transform into constituent quarks with mass and magnetic moment. The last step is the formation of the hadron-antihadron pair moving apart, as a results of the competition between the available kinetic energy,  $T = \sqrt{q^2} - E_{Th}$  and the confinement energy,  $k_s/2R_{pp}$ , where  $k_s \simeq 1 \text{ GeV/fm}$  is the confinement elasticity constant and  $R_{pp}$  is the distance between the centers of the forming hadron and antihadron. When the velocity is very small, a bound state can be formed with dimensions up to hundreds of fm.

In Ref. [12] the comparison with the experimental data was limited, due to the few measurements especially in the time-like region. Recently an important amount of data on proton and neutron FFs in the time-like region has been made available by the BESIII Collaboration. In next section we

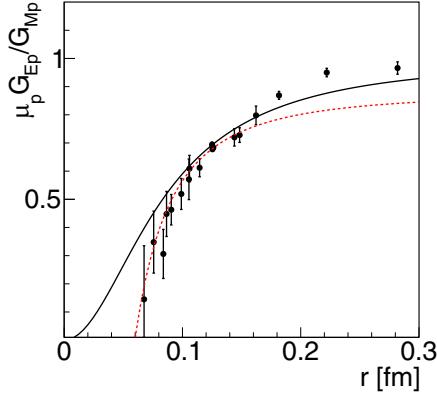


FIG. 1. Proton FF ratio as a function of the internal distance seen by the virtual photon. The points are from Ref. [11] and references therein. The dashed red line is a  $Q^2$ -linear fit of the highest  $Q^2$  points, the solid black line is the monopole fit, Eq. (4).

compare the dynamical evolution of the baryonic system, as predicted by the model, with the present world data set.

### III. THE SPACE STRUCTURE OF THE PROTON

In the space-like region, polarization measurements provide information on the electric to magnetic FF ratio. Instead of the usual variable  $Q^2$ , we report the data from the JLab-GEp experiment [11] as a function of  $r$ , the scale length associated to the wavelength  $\lambda$  of the virtual photon with squared four-momentum  $Q^2$ , i.e.,

$$r [\text{fm}] = \lambda = \hbar c / \sqrt{Q^2} = 0.197 [\text{GeV fm}] / \sqrt{Q^2} [\text{GeV}], \quad (3)$$

where small values of  $r$  correspond to large values of  $Q^2$ .

The internal distances covered by the kinematics where data exist extend to very small nucleon sizes, about two orders of magnitude smaller than the nucleon dimension. At the other extreme, very small values of  $Q^2$ , corresponding to large values of  $r$ , will prevent the virtual photon to resolve the proton structure. By definition, the electric and magnetic FFs at  $Q^2 = 0$  have to coincide with the electric charge (one, in units of  $e$  charge) and with the magnetic moment  $\mu_p$ , respectively.

The FF ratio  $\mathcal{R} = \mu_p G_{Ep} / G_{Mp}$ , shown in Fig. 1 as a function of  $r$ , can be parametrized by a straight line or the monopole form of mass  $m_r$ :

$$\mathcal{R} = \mu_p \frac{G_{Ep}}{G_{Mp}} = \left(1 + \frac{Q^2}{m_r^2}\right)^{-1} \simeq \left(1 + \frac{0.197^2}{m_r^2 r^2}\right)^{-1}, \quad (4)$$

where, following Eq. (3),  $r$  is in units of fm. The proton FF ratio decreases regularly, showing definitely a suppression of  $G_{Ep}$  compared to  $G_{Mp}$ . It can be reasonably reproduced by Eq. (4) with  $m_r^2 = 5.6 \text{ GeV}^2$  and approaches to zero, within the errors, for  $r \leq 0.06 \text{ fm}$ . Such a length corresponds to the largest value of  $Q^2$  measured by the GEp experiment. An extended program of measurements up to  $Q^2 = 15 \text{ GeV}^2$  is planned at Jefferson Laboratory, following the energy upgrade [15], with the main aim to investigate if the ratio will cross zero and eventually become negative. The smooth  $Q^2$ -decreasing behavior of  $\mathcal{R}$  agrees with the model of Ref. [12].

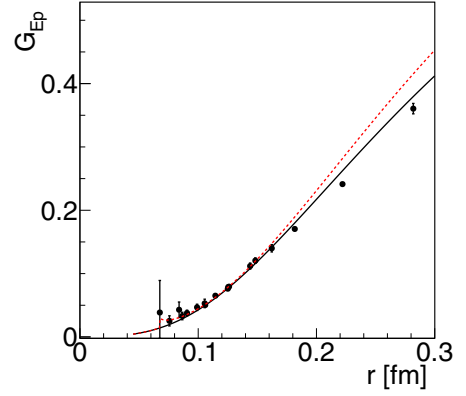


FIG. 2. Electric proton FF as a function of the internal distance  $r$  seen by the virtual photon. Notations as in Fig. 1.

Moreover,  $\mathcal{R}$  approaching to zero at large  $Q^2$ , can be interpreted as due to the vanishing of the electric FF for internal distances corresponding to the screening region. A linear  $Q^2$  extrapolation of the high- $Q^2$  (low  $r$ ) points, represented by the red dashed line in Fig. 1, allows us to set the size of this region at  $\leq 0.06 \text{ fm}$ . At larger  $Q^2$  values the model predicts that the ratio stays very small.

In the light of the structures observed in the time-like region, as well as of the inhomogeneity in the electromagnetic density originated by the different configurations participating in the hadron-antihadron formation, one may expect to observe irregularities instead of a smooth behavior of the ratio. One reason can be that these structures have been associated to the interference among phenomena occurring at different scales or to rescattering effects related to the imaginary parts of the amplitudes. In this case, they should be suppressed in the space-like region, where FFs are real, appearing preferentially in the time-like region, where FFs are complex, with nonvanishing imaginary parts due to unitarity. Another reason is that these structures, being similar in the individual FFs, may be canceled in the FF ratio.

The Rosenbluth separation (unpolarized  $ep$  elastic scattering cross section measurements at fixed  $Q^2$  at different angles) allows to extract separately  $G_{Ep}$  and  $G_{Mp}$  but only at small  $Q^2$ . At large  $Q^2$  the term corresponding to the electric contribution to the cross section is hidden as it is of the same order as the experimental errors, making doubtful the extraction of the individual FFs. Precise polarization measurements allow to extract only the FF ratio. But one can derive the electric FF from the ratio, assuming that the magnetic FF is well determined from the Rosenbluth measurements, since the magnetic driven contribution to the unpolarized cross section is dominant.  $G_{Mp}$  has been measured up to  $Q^2 = 30 \text{ GeV}^2$  and it shows indeed some deviation from a dipole, with a dip around  $Q^2 = 0.2 \text{ GeV}^2$  and a bump around  $Q^2 = 3 \text{ GeV}^2$ .

Calculating  $G_{Ep}$  from the ratio  $\mathcal{R}$ , with the help of the fit from Ref. [16], that gives a reliable description of the  $G_{Mp}$  data, one finds a smooth behavior for the electric FF, with no evident structures as shown in Fig. 2.

The recent  $G_{Ep}$  data, collected at very small  $Q^2$  for determining the proton radius, can also be plotted as a function

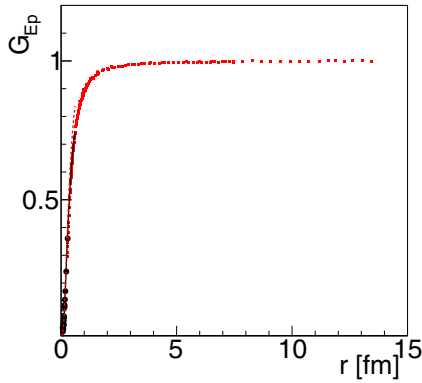


FIG. 3. Electric FF of the proton as a function of the internal distance in fm, as seen by the virtual photon. The red points are from Ref. [19], other notations as in Fig. 2.

of  $r$ . Figure 3 shows that the resolving power of a photon of such a small four-momentum squared is very large, up to 15 fm. Therefore one may wonder how a photon with such four-momentum squared can give a meaningful measurement of the proton dimension, which is about 20 times smaller, how well it can ‘see’ the proton size, and discriminate a value between 0.84–0.87 fm, corresponding to what is needed to solve the so-called ‘proton puzzle’. This argument corroborates the finding and the quantitative discussion of Refs. [17,18].

Following this discussion, one can predict that the measurements of proton FFs at large  $Q^2$  values will not bring additional information on the proton structure, confirming a very small or vanishing electric FF. The efforts to perform measurements at  $Q^2 \rightarrow 0$  with higher precision is also a nonsense: the smaller is  $Q^2$  the less precisely the photon will see the proton dimension.

#### The space structure of the neutron

The values of the neutron electric FF in the space-like region are small with respect to unity, as it vanishes at  $Q^2 = 0$  which corresponds, by definition, to the neutron electric charge. It has usually been considered uniformly equal to zero, but since that precise data have been obtained, also using the Akhiezer-Rekalo polarization method [2,3], a more complicated picture appeared. The data on the electric neutron FF (Fig. 4), although less precise than those of the proton, and extending to a shorter  $Q^2$  range, show an increase at small  $Q^2$ , eventually a plateau between 0.2 and 0.8 fm, and then a decrease to zero at large  $Q^2$  (small  $r$ ). The upper scale in Fig. 4 indicates the wavelength of the virtual photon, corresponding to its four-momentum squared, i.e., the internal distance that can be probed. At large  $Q^2$ , by construction, the parametrization [20] goes as  $Q^{-2}$ . The data show the tendency to reach a zero well above  $Q^2 = 4 \text{ GeV}^2$ , i.e., for internal distances  $r \ll 0.2 \text{ fm}$ .

The magnetic FFs, normalized to the corresponding magnetic moments, are similar for neutron and proton, essentially following the standard dipole behavior:

$$G_D = (1 + Q^2/0.71 \text{ GeV}^2)^{-2}. \quad (5)$$

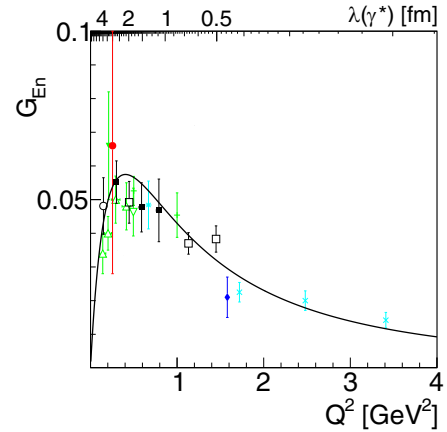


FIG. 4. Electric form factor of the neutron as a function of the momentum transfer square from Refs. [21] (solid blue diamond), [22] (cyan cross), [23] (cyan asterisk), [24] (green triangle), [25] (green cross), [26] (open green down triangle), [27] (solid green down triangle), [28] (open black square), [29] (solid black square), [30] (open solid circle), [31] (red circle). The line is the parametrization from Ref. [20]. The upper scale shows the corresponding wavelength of the virtual photon.

In Fig. 5 the magnetic FFs (normalized to the corresponding magnetic momenta) are shown as functions of  $r$  for neutron (black squares) and proton (red circles). The data are selected from the compilation of Ref. [1]. At small  $Q^2$  (large  $r$ ) the FFs values approach unity. The behavior at the smallest values of  $Q^2$  is driven by the very precise experiments that had the aim to measure the proton radius [19].

#### IV. THE TIME STRUCTURE OF PROTONS, NEUTRONS AND HYPERONS

Let us focus on the process  $e^+e^- \rightarrow p\bar{p}$ . As recalled in Sec. II, FFs in the annihilation region carry information on the time evolution of the spatial distribution of the charge which is created at the annihilation point. The charge is carried by

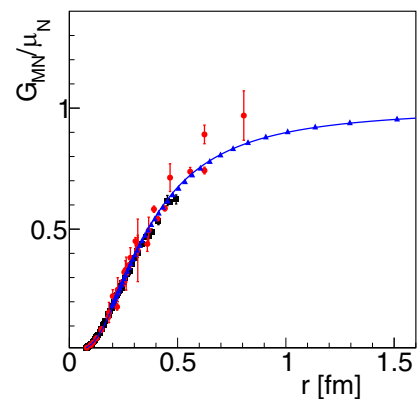


FIG. 5. Magnetic FF of the proton (black squares) and of the neutron (red circles) normalized to the correspondent magnetic moment, as a function of the internal distance  $r$  in fm. The blue triangles are the  $G_{Mp}$  data extracted from Ref. [19] (spline option). The blue line is the dipole function.

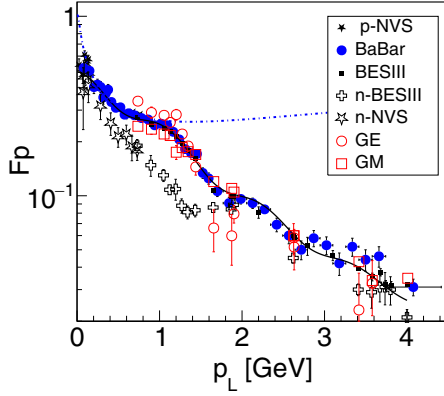


FIG. 6. Time-like effective FF of the nucleon as a function of the relative momentum  $p_L$ : generalized (open black crosses), electric (open red circles), and magnetic FF of the proton (open squares) [7]. The black solid line is the six parameter fit from Ref. [34]. The blue dashed line is the expected generalized to a constant cross section  $\sigma = 0.87$  mb, corresponding to  $|G_E| = |G_M| = 1$ . The neutron FF is shown as open black symbols, stars from Ref. [10] and crosses from Ref. [9].

the bare quarks that evolve to dressed quarks and eventually diquarks, till the hadron-antihadron pair formation. It may be interesting to investigate which time scale is related to these stages. According to Ref. [12], the different phases of the hadron formation are related to the time of evolution of the system and to the distance  $D$  between the forming hadron and antihadron.

The cross section of the process  $e^+e^- \rightarrow p\bar{p}$  has been measured by the CMD-3 experiment at Novosibirsk [10,32], by the BaBar experiment at SLAC [5,6] and by the BESIII experiment at Beijing in several works, using initial state radiation [8,33] and the beam energy scan method [7]. The data show indeed a region where the cross section is compatible with a structureless proton, see Fig. 6. In Ref. [34] it was found that not only the effective FF, that is the square root of a combination of the moduli squared of the electric and magnetic FFs but also the modulus of their ratio shows marked oscillations, that have to be mostly attributed to the electric FF.

In Fig. 6 the effective nucleon FF is plotted as a function of the modulus of the relative three-momentum of the produced nucleons in the laboratory system  $p_L$ . Near threshold the proton and neutron FFs are comparable, as well as above  $p_L = 2$  GeV. Regular oscillations for the proton FF, when plotted as a function of this variable, are well reproduced by the six parameter fit given in Ref. [34]. The neutron FF is smaller than the proton FF in the region  $0.4 \leq p_L \leq 1.4$  GeV, it is about constant for  $1.4 < p_L \leq 2$  GeV and then reaches the proton FF values from  $p_L \simeq 2$  GeV on.

The moduli of the electric and magnetic proton FFs are also reported in Fig. 6. It is clear that  $|G_{Mp}|$  has a smooth behavior, whereas  $|G_{Ep}|$  seems to follow the behavior of the effective neutron FF, with a steep decrease and a plateau in the region  $1.6 \leq p_L \leq 2.6$  GeV. At large energies all FFs converge towards common, very small and real values.

The time-like FF has been precisely measured by the BESIII experiment not only for neutrons [9], but also for  $\Lambda$  in

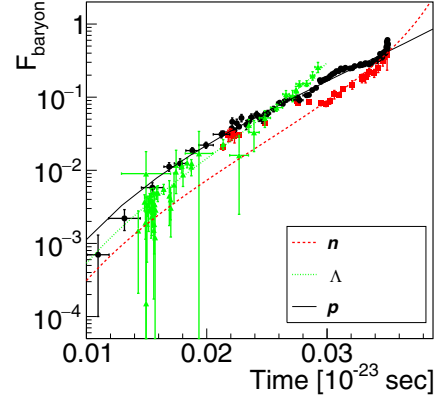


FIG. 7. Time scale of FFs as a function of the time scale for neutron [9,10] (red squares), proton [5,6,33] (black circles), and  $\Lambda$  [35–37] (green triangles).

Ref. [35] overlapping with the data from BaBar experiment [36], and at higher energies [37].

The transferred momentum square can be related to the time evolution from the annihilation point. In the time-like region, and in CMS, only the energy component of the four-momentum is different from zero. Then the energy scale can be converted in time scale

$$t [\text{sec}] = \frac{\hbar c}{q_0} = \frac{0.0658 \times 10^{-23} [\text{GeV s}]}{q_0 [\text{GeV}]} \quad (6)$$

In Fig. 7 we can see that the time scale corresponding to the data is in the range  $(1-3) \times 10^{-2}$  in units of  $10^{-23}$  s, which is the characteristic time for the light to travel through the proton.

Three main trends can be seen: a steep decreasing near threshold (the threshold corresponds to the largest time), a plateau that is more evident for the neutron and at comparable time for the proton, and a dipole (or tripole) behavior at large  $q^2$  (small times). The  $\Lambda$  baryon follows a similar trend, the threshold and the plateau occurring at shorter times. This can be attributed to the larger mass of the  $\Lambda$  and, at the quark level, to the need to create a strange quark-antiquark pair.

The hadron and the antihadron move apart when the kinetic energy  $T = q_0 - 2M_N$  exceeds the confinement energy,  $(k_s/2)R_{pp}$ , where  $k_s = 1$  GeV/fm is the strength of the color force attraction. Note that in the threshold region, the dimension of the system can reach hundreds of fm.

## V. CORRELATION OF FFs FOR NEUTRON, PROTON AND $\Lambda$

The fact that the three regions, corresponding to three regimes in the evolution of the baryonic system, are common to different baryons implies some correlation among the FFs. To make evident such correlation, in Fig. 8 the effective neutron FF is plotted in the ordinate and the proton FF measured at the same  $p_L$  in the abscissa (red triangles). The proton FF has also been calculated from the six-parameter proton data fit of Ref. [34] (black asterisks), especially useful when data are not available at the same  $p_L$ . The long dashed line is drawn to guide the eyes. The dashed red line corresponds to  $F_n = F_p$ .

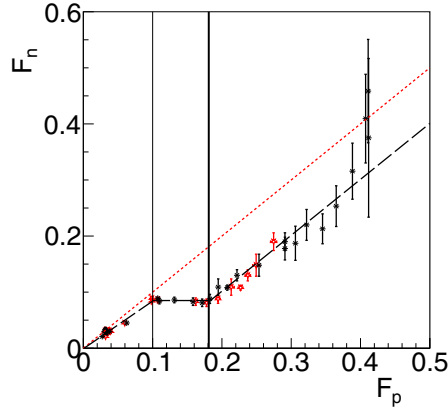


FIG. 8. Neutron-proton effective FF correlation at corresponding  $p_L$  (red open triangles). When the data are not present at the same  $p_L$ , the six-parameter fit from Ref. [34] is used for the proton (black asterisks). The red dashed line shows  $F_n = F_p$ , the black long dashed line is drawn to drive the eyes. The thin and thick black solid lines delimit the region of discontinuity (see text).

Three regimes and two regions where the proton and neutron FF are strongly correlated with two breaking points indicated by the thin and thick vertical lines, are evident. The first one corresponds to  $(F_p, F_n) \simeq (0.1, 0.085)$ , occurring around  $p_L = 1.3$  GeV, ( $q^2 = 4.7$  GeV<sup>2</sup>) and the second one at  $(F_p, F_n) = (0.18, 0.085)$ , occurring around  $p_L = 1.9$  GeV, ( $q^2 = 5.7$  GeV<sup>2</sup>). Note that the threshold corresponds to the right top of the figure and the large  $q^2$  region to the points gathered near the origin.

Figure 9 shows, in addition to those of the neutron, the  $\Lambda$  baryon data in logarithmic scale. The data for the  $\Lambda$  do not have the same quality. Still, they show a very similar behavior, where the change of regime occurs around  $(F_p, F_\Lambda) \simeq (0.025, 0.018)$ , i.e.,  $p_L = 2.4$  GeV, ( $q^2 = 8.4$  GeV<sup>2</sup>) (thin green dash-dotted line) and the second one at  $(F_p, F_\Lambda) = (0.08, 0.018)$  (thick green dash-dotted line), i.e.,  $p_L = 5.1$  GeV, ( $q^2 = 14.2$  GeV<sup>2</sup>). This can be associated to the production of strange quark-antiquark pairs that are heavier and therefore correspond to a shorter time for their production and recombination.

## VI. CONCLUSIONS

We have shown peculiar features of the baryon FF data which corroborate the picture suggested in Ref. [12] for the description of the baryon structure. Such picture appears coherently in scattering and annihilation reactions.

In particular, the recent data are consistent with a neutral region at very small distances, that is responsible for a steeper decrease of the electric FF compared to the magnetic one. This region can be determined from the elastic scattering data to

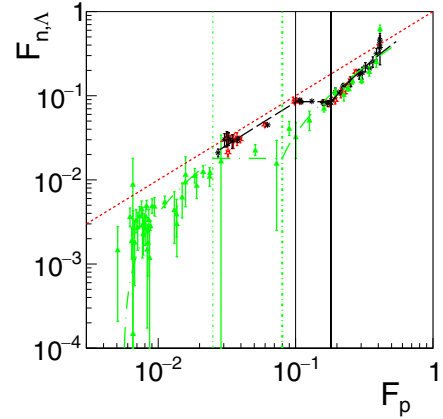


FIG. 9. Neutron-proton and  $\Lambda$ -proton correlation (solid green triangles). The dash-dotted thin and thick lines delimit tentatively the discontinuity region. Other notations as in Fig. 8.

have a size smaller than about 0.06 fm. If it is the case, one can predict that the FF ratio will stay small around zero. This prediction will be soon confirmed or disproved by the planned experiments at Jefferson Laboratory.

The interval of time of  $(0.01-0.03) \times 10^{-23}$  s running from the annihilation point to the hadron-antihadron formation gives a very precise inside scale of the process. Even more precisely one can situate the transition from the point-like quark state to the detectable hadron, through a complex state of different configurations. Among them, there are overlapping configurations, occurring with different probabilities, including diquarks, at the level of  $(0.028-0.035) \times 10^{-23}$  s for nucleons and slightly shorter for strange baryons:  $(0.018-0.022) \times 10^{-23}$  s. This stage corresponds to the expansion of the quark and gluon system created from the  $e^+e^-$  annihilation to constituent quarks getting a mass and a dimension after absorbing gluons. A similar behavior, but with a different scale between hyperons and nucleons can be understood, by the different mass of the involved quarks. In the instanton picture, in Ref. [14], a classification of the currents and a mass scale for the formation of the different hadrons were suggested, based on the dependence on the quantum numbers of the interaction with the vacuum field.

It is also interesting to notice that the size of the system near threshold, when, due to the competition of the between the kinetic and the confinement energies, the relative velocity of the formed hadron and antihadron leaving the interaction zone is very small, can reach hundreds of fm.

## ACKNOWLEDGMENTS

We acknowledge Andrea Bianconi for interesting discussions and advices. We are grateful to Victor Kim for continuous interest in this topics. Thanks are due to Yury Bystritskiy for useful discussions.

[1] S. Pacetti, R. Baldini Ferroli, and E. Tomasi-Gustafsson, *Phys. Rep.* **550–551**, 1 (2015).

[2] A. Akhiezer and M. Rekalov, *Dokl. Akad. Nauk Ser. Fiz.* **180**, 1081 (1968) [*Sov. Phys. Dokl.* **13**, 572 (1968)].

- [3] A. I. Akhiezer and M. P. Rekalov, *Fiz. Elem. Chast. Atom. Yadra* **4**, 462 (1973) [*Sov. J. Part. Nucl.* **4**, 277 (1974)].
- [4] A. Bianconi and E. Tomasi-Gustafsson, *Phys. Rev. Lett.* **114**, 232301 (2015).
- [5] J. Lees *et al.* (BaBar Collaboration), *Phys. Rev. D* **88**, 072009 (2013).
- [6] J. Lees *et al.* (BaBar Collaboration), *Phys. Rev. D* **87**, 092005 (2013).
- [7] M. Ablikim *et al.* (BESIII Collaboration), *Phys. Rev. Lett.* **124**, 042001 (2020).
- [8] M. Ablikim *et al.* (BESIII Collaboration), *Phys. Lett. B* **817**, 136328 (2021).
- [9] M. Ablikim *et al.* (BESIII Collaboration), *Nat. Phys.* **17**, 1200 (2021).
- [10] R. R. Akhmetshin *et al.* (CMD-3 Collaboration), *Phys. Lett. B* **794**, 64 (2019).
- [11] A. J. R. Puckett *et al.* (GEP Collaboration), *Phys. Rev. C* **96**, 055203 (2017); **98**, 019907 (2018).
- [12] E. A. Kuraev, E. Tomasi-Gustafsson, and A. Dbeyssi, *Phys. Lett. B* **712**, 240 (2012).
- [13] A. Bianconi and E. Tomasi-Gustafsson, *Phys. Rev. C* **95**, 015204 (2017).
- [14] A. I. Vainshtein, V. I. Zakharov, V. A. Novikov, and M. A. Shifman, *Fiz. Elem. Chast. Atom. Yadra* **13**, 542 (1982) [*Sov. J. Part. Nucl.* **13**, 224 (1982)].
- [15] E. J. Brash *et al.*, Large acceptance proton form factor ratio measurements up to  $14.5 \text{ GeV}^2$  using recoil-polarization method (2009), [https://userweb.jlab.org/~bogdanw/gep\\_u.pdf](https://userweb.jlab.org/~bogdanw/gep_u.pdf).
- [16] E. J. Brash, A. Kozlov, S. Li, and G. M. Huber, *Phys. Rev. C* **65**, 051001(R) (2002).
- [17] S. Pacetti and E. Tomasi-Gustafsson, *Eur. Phys. J. A* **56**, 74 (2020).
- [18] S. Pacetti and E. Tomasi-Gustafsson, *Eur. Phys. J. A* **57**, 72 (2021).
- [19] J. C. Bernauer *et al.* (A1 Collaboration), *Phys. Rev. C* **90**, 015206 (2014).
- [20] J. J. Kelly, *Phys. Rev. C* **70**, 068202 (2004).
- [21] B. S. Schlimme, P. Achenbach, C. A. Ayerbe Gayoso, J. C. Bernauer, R. Bohm *et al.*, *Phys. Rev. Lett.* **111**, 132504 (2013).
- [22] S. Riordan, S. Abrahamyan, B. Craver, A. Kelleher, A. Kolarkar *et al.*, *Phys. Rev. Lett.* **105**, 262302 (2010).
- [23] J. Bermuth *et al.*, *Phys. Lett. B* **564**, 199 (2003).
- [24] E. Geis *et al.* (BLAST Collaboration), *Phys. Rev. Lett.* **101**, 042501 (2008).
- [25] G. Warren *et al.* (Jefferson Lab E93-026), *Phys. Rev. Lett.* **92**, 042301 (2004).
- [26] H. Zhu *et al.* (E93026 Collaboration), *Phys. Rev. Lett.* **87**, 081801 (2001).
- [27] I. Passchier, R. Alarcon, T. S. Bauer, D. Boersma, J. F. J. van den Brand *et al.*, *Phys. Rev. Lett.* **82**, 4988 (1999).
- [28] B. Plaster *et al.* (Jefferson Laboratory E93-038 Collaboration), *Phys. Rev. C* **73**, 025205 (2006).
- [29] D. Glazier, M. Seimetz, J. Annand, H. Arenhovel, M. Ases Antelo *et al.*, *Eur. Phys. J. A* **24**, 101 (2005).
- [30] C. Herberg, M. Ostrick, H. Andresen, J. Annand, K. Aulenbacher *et al.*, *Eur. Phys. J. A* **5**, 131 (1999).
- [31] T. Eden, R. Madey, W. M. Zhang, B. D. Anderson, H. Arenhovel *et al.*, *Phys. Rev. C* **50**, R1749(R) (1994).
- [32] R. Akhmetshin *et al.* (CMD-3 Collaboration), *Phys. Lett. B* **759**, 634 (2016).
- [33] M. Ablikim *et al.* (BESIII Collaboration), *Phys. Rev. D* **91**, 112004 (2015).
- [34] E. Tomasi-Gustafsson, A. Bianconi, and S. Pacetti, *Phys. Rev. C* **103**, 035203 (2021).
- [35] M. Ablikim *et al.* (BESIII Collaboration), *Phys. Rev. D* **97**, 032013 (2018).
- [36] B. Aubert *et al.* (BaBar Collaboration), *Phys. Rev. D* **76**, 092006 (2007).
- [37] M. Ablikim *et al.* (BESIII Collaboration), *Phys. Rev. D* **104**, L091104 (2021).